



## Research Paper

## Environment friendly dual-frequency ultrasonic exfoliation of few-layer graphene



Anastasia V. Tyurnina<sup>a,\*</sup>, Justin A. Morton<sup>b</sup>, Tungky Subroto<sup>a</sup>, Mohammad Khavari<sup>b,d</sup>, Barbara Maciejewska<sup>d</sup>, Jiawei Mi<sup>c</sup>, Nicole Grobert<sup>d,e</sup>, Kyriakos Porfyrakis<sup>f</sup>, Iakovos Tzanakis<sup>b</sup>, Dmitry G. Eskin<sup>a,g</sup>

<sup>a</sup> Brunel Centre for Advanced Solidification Technology, Brunel University London, Kingston Lane, UB8 3PH, UK

<sup>b</sup> School of Engineering, Computing and Mathematics, Oxford Brookes University, College Ct, Wheatley, Oxford, OX33 1HX, UK

<sup>c</sup> Department of Engineering, University of Hull, Cottingham Rd, Hull, HU6 7RX, UK

<sup>d</sup> Department of Materials, University of Oxford, Parks Rd, Oxford, OX1 3PH, UK

<sup>e</sup> Williams Advanced Engineering, Grove, Oxfordshire, OX12 0DQ, UK

<sup>f</sup> Faculty of Engineering and Science, University of Greenwich, Park Row, London, SE10 9LS, UK

<sup>g</sup> Tomsk State University, 36 Lenin. Ave., Tomsk, 634050, Russia

## ARTICLE INFO

## Article history:

Received 11 August 2021

Received in revised form

11 September 2021

Accepted 15 September 2021

Available online 22 September 2021

## Keywords:

Graphene

Acoustic pressure

Ultrasonic exfoliation

Shock wave emission

## ABSTRACT

Ultrasound-aided liquid phase exfoliation (ULPE) of graphene in pure water is environment-friendly. Two limiting factors of ULPE are the non-uniform thickness of few-layer graphene (FLG) and a relatively low graphene yield. Here we describe ULPE in water that enables us to produce FLG flakes with a thickness of 3 layers and the flake sizes exceeding  $1 \mu\text{m}^2$  in just 2 h. This process is based on using a combination of two ultrasound sources of high and low frequencies: 1174 kHz and 20 kHz. Two different frequencies generate a wider population and size distribution of cavitation bubbles that act through a number of mechanisms towards the exfoliation of graphene. For the first time ULPE was characterized by acoustic measurements. Results show that a high graphene yield (10%) can be achieved. This study demonstrates that the use of a dual frequency ultrasonic source and control of acoustic pressure is critical in optimizing the quality and yield of the cavitation assisted LPE of graphene in pure water. It is suggested that the width of the acoustic pressure peak reflecting shock-wave emissions can be used as an indicator of ULPE completeness, opening for the first time a way of in-situ monitoring of the process.

© 2021 The Author(s). Published by Elsevier Ltd. This is an open access article under the CC BY license (<http://creativecommons.org/licenses/by/4.0/>).

## 1. Introduction

Since its discovery [1], graphene has established itself as a material with various advanced properties: excellent electrical and thermal conductivity, optical and mechanical characteristics [2–4]. Although its potential applications are virtually unlimited and cover many fields (energy [5], electronics [6], medicine [7], sports [8], etc. [9]), mass production of graphene remains a challenging task [10–12]. Among different methods of graphene fabrication, liquid phase exfoliation (LPE) is the most promising for some graphene industrial applications due to the feasibility to obtain monolayer or few-layer defect-free graphene in the form of liquid suspensions, inks, or dispersions, stable and scalable for mass

production [13,14]. However, in addition to a low graphene yield [14,15] and nonuniformity (size and thickness) of as-produced few-layer graphene (FLG) flakes [14,16], the main drawback of the LPE approaches is the necessity of expensive, hazardous and harmful solvents and the excessive use of surfactants [16–18]. Though these chemicals help to disperse and stabilize the FLG flakes in the solution [19–21], they are at the same time toxic to the environment and contaminate the FLG flakes. Therefore, graphene production is not only costly, but also suffer from environmental problems due to the huge amount of waste generated during graphene manufacturing. Economic and environmental concerns became an obstacle for industries to benefit from graphene in full measure. It is expected that in the next few years the demand for graphene will increase to over 10 thousand tons per year, making the current total global capacity of manufacturers highly insufficient [22]. Several LPE studies have already pointed out the importance of searching for a green solvent [13,14,16], with the use of water appealing as an

\* Corresponding author.

E-mail address: [Anastasia.Tyurnina@brunel.ac.uk](mailto:Anastasia.Tyurnina@brunel.ac.uk) (A.V. Tyurnina).

eco-friendly medium for graphene LPE [14,23]. However, most of these studies combined water with various organic surfactants [21,24] or used weak aqueous alkaline solution [25]. These approaches require an additional purification step in the fabrication process [20,26], if removing the surfactant proves challenging [14].

Recently, it was shown that water can be used as a dispersant after LPE [23], but, to the best of our knowledge, only few reports did exfoliation in just pure water [27,28]. Previously, the water solvent was considered as a poor medium for LPE of graphene, due to the mismatch of chemical parameters (mainly surface tension [21]) and high hydrophobicity [25], both considered to play the key role in graphite exfoliation and dispersion [21,23]. Later it was demonstrated that graphene (unlike graphite) was more likely to be hydrophilic to water [29], and has also shown theoretically that solvent's surface energy or Hansen solubility parameters did not need to be close to those of graphene [13]. These recent advances suggested that the interaction between water and the graphitic surface had been underestimated.

This work reports the synthesis of unfunctionalized, non-oxidized graphene applying the ultrasound-assisted method by LPE of a graphite powder in pure water. Previously, we have shown a significant role of choosing the ultrasonic frequency for the quality and yield of LPE in pure water [27]. In this study we took a further step and look at the combination of two sources (high- and low-frequency) in ultrasonic LPE (ULPE) of FLG and supplement the structure characterisation of produced FLG with acoustic characterisation of the process.

## 2. Materials and methods

Graphite powder (GP) purchased from Alfa Aesar (LOT: B08Z019) was used as an initial source for graphene exfoliation in pure deionized water (DIW) supplied by Lab Unlimited Carl Stuart group. The average size of the initial GP was about 70  $\mu\text{m}$  as per manufacturer's specification. Commercially produced graphene (Eau de Graphene, CW-G101A1-16) in water was purchased for comparing the characteristics such as size, thickness and quality with those of FLG flakes produced in our study. In all experiments, 60 mg of GP was added into a 50-mm diameter clear PVC beaker filled with 150 ml of DIW and stirred in gently by a Teflon spoon prior to ultrasonic (US) treatment.

From the top and bottom of the beaker different types of US sources were applied. A schematic view of our ULPE set-up is shown in Fig. 1a. From the top, a 20-mm/24-kHz Ti sonotrode (marked as 1) was attached to an L500/5–20 Sonic Systems ultrasonic processor, with a max peak-to-peak amplitude of 30  $\mu\text{m}$  (designated as Lf – low frequency). It was immersed into the beaker centre, 2-mm deep from the liquid surface. The second US source was applied from the bottom of the beaker (marked as 2). This was a multi-frequency membrane transducer (Meinhardt Ultrasonics) with a Ti diaphragm (50 mm in diameter, equal to the beaker diameter) that was used at 1174 kHz (designated as Hf – high frequency). Both transducers were used at 50% of their maximum input power.

The following four different US regimes denoted with (1–4) were tested for the exfoliation, with the total ULPE time kept at 2 h for each case. (1) Both sources worked simultaneously, abbreviated as “Hf&Lf together”. (2) US sources alternate with 10 min interval, further defined as “10 min/Hf–10 min/Lf”. (3) A 1 h Lf processing followed by 1 h Hf processing (“1 h/Lf–1 h/Hf”). (4) A 1 h Hf processing followed by 1 h Lf processing (“1 h/Hf–1 h/Lf”). Results obtained in the previous work using the same settings but with a single, either Lf or Hf, source were used for comparison [27].

The cavitation intensity in the liquid was monitored using two advanced calibrated acoustic sensors: a 10  $\mu\text{m}$  diameter fibre-optic

hydrophone (FOH, Precision Acoustics Ltd) calibrated between 1 and 30 MHz and a 4 mm diameter needle hydrophone (NH, Precision Acoustics Ltd) calibrated in the National Physical Laboratory (UK) from 8 to 400 kHz. The purpose of using these two different sensors was capturing the acoustic emission from a broad range of frequencies associated to the cavitating and collapsing bubbles and corresponding shock wave emissions (FOH) [30] as well as acoustic emissions from sound waves including harmonics, ultra and sub-harmonics generated by the driving frequencies of the Lf (NH) and Hf (FOH) sources [31]. Acoustic signals captured by both acoustic sensors were converted into raw voltage signal and recorded by an external digital oscilloscope device (PicoScope 3000 series). This enabled real-time signal monitoring of the cavitation activities. A set of 60 signals were captured within a signal acquisition window (time gate) of 2 ms, resulting in total of 120 ms. The signals were acquired with a high sampling rate of 500 MS/s, and at least three sets of measurements were performed per data point to observe the statistical behaviour.

The acoustic pressure was obtained by converting the raw voltage signal data using Fast Fourier Transform (FFT) and applying the sensitivity function of the acoustic sensor calibrated at different frequencies. An in-house MATLAB code was developed and used for the deconvolution process following the procedure described elsewhere [30]. The cavitation activities in the frequency-domain could be observed through two different ways. The pressure vs. frequency results were obtained by converting time-domain signals with the aforementioned procedure [32] within the calibrated frequency range of each cavitation sensor. Meanwhile, the broadband spectra were obtained by transforming the raw voltage signal to the time-domain data within the PicoScope. To assess the broadband activities of the cavitation, two frequency ranges were used; to observe the lower frequency regime, a window of frequency up to 400 kHz was used (with bandwidth resolution of ~61 Hz) for the NH, while a broadband window up to 5 MHz (with bandwidth resolution of ~610 Hz) was used to monitor all activities captured by the FOH.

The acoustic pressure measurements were taken by submerging the hydrophones at opposite ends of the beaker, with the sensor tips 1 cm below and approximately 2 cm sideways from the Lf sonotrode tip (as shown in Fig. 1a by white crosses). General noise intensity that was subtracted from the acoustic pressure spectra as explained in Ref. [32] was detected for 3 different configurations: Hf, Lf and their combination (i.e., Hf&Lf together). Each measurement was taken at different stages of the process: in DIW, immediately after adding the GP to DIW, and each 10 min thereafter until the end of a 2 h LPE process.

The temperature of the solution was monitored by a K-type standard thermocouple with an RS 52 Digital Thermometer (marked as 3 in Fig. 1a). To maintain as-prepared mixture at the same temperature, cooling arrangement was used to surround the PVC beaker and allow for stabilizing the temperature at  $45 \pm 3$  °C.

After 2 h of US treatment, an exfoliated sample of FLG flakes in DIW was centrifuged (CF) at 1500 relative centrifugal force (rcf) for 30 min by a Heraeus, type Labofuge 400R system. The upper part of the CF solution (about 25 ml) was collected at once to a precleaned glass vial in order to prepare several different supernatant samples for the following advanced characterizations.

UV–vis spectroscopy was carried out immediately after centrifugation to prevent measuring the spectra when FLG flakes in the solution started agglomerating. A Hewlett Packard 8453 instrument was used to collect the spectra in the wavelength range 220–800 nm, which was enough to detect the graphene and potential graphene oxide (GO) related peaks (expected at 270 [33] and 230 nm [34], respectively). For that, a certain amount of the CF solution was poured into a 3.5-ml Cole-Palmer quartz cuvette, with

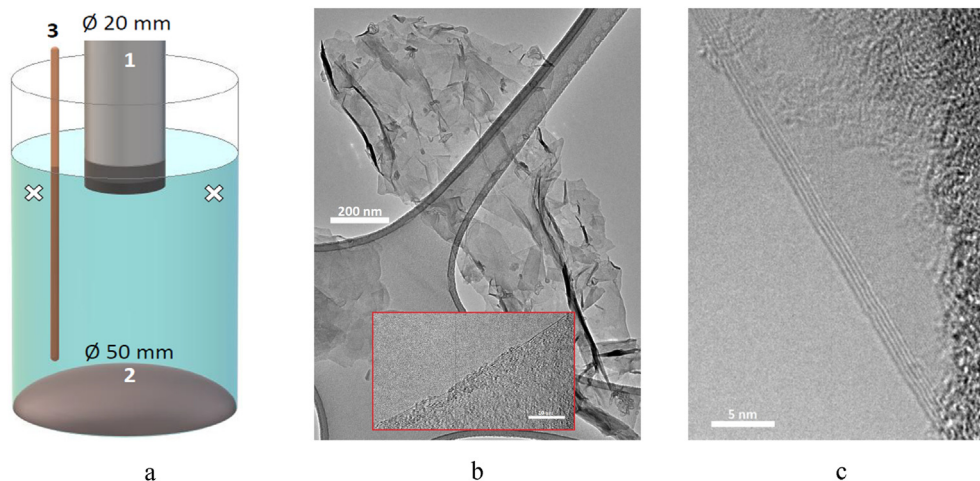


**Fig. 1.** (a) Schematic view of the experimental set-up with 2 US sources for graphene exfoliation in DIW. (1) 20-mm/24-kHz sonotrode (Lf) applied from the top of the beaker, (2) 50-mm/1174-kHz membrane (Hf) applied from the bottom and (3) thermocouple. US sources diameters are indicated by symbol  $\varnothing$ . The white crosses mark the NH and FOH hydrophones positions during acoustic pressure measurement; (b) TEM image of low and high resolution (HR, inset) of a typical FLG flake obtained after LPE configuration called as “Hf&Lf together”; (c) higher magnification of HR TEM of another 5Ls flakes edge. (A colour version of this figure can be viewed online.)

a path length of 10 mm, and measured with an acquisition time of 10 s.

Consequently, a drop of the CF solution was casted onto a pre-cleaned Si/SiO<sub>2</sub> (300 nm) surface and dried at room temperature (RT) within a ducted fume cupboard prior to Raman investigation. Another 3 drops were put onto holey-carbon-coated copper grids (300 mesh) for transmission electron microscopy (TEM) investigation and also dried at RT. An InVia Raman (Renishaw) spectroscopy system with Modu-Laser working at an excitation wavelength of 514 nm was used to confirm the FLG structure, to verify the number of layers (NLs) by checking the 2D/G intensity ratio, presence of defects from the intensity ratios D/G and D/D', and to trace the FLG structure quality after US process (Fig. 2). The laser spot size was  $\sim 2 \mu\text{m}$  and the laser power was 0.2 mW. Raman spectra of 23–30 random flakes were registered for each sample in the range from 1200 to 3100 cm<sup>-1</sup>. Data collection was made under 50  $\times$  magnification, the acquisition time was adjusted to have a reasonable signal/noise ratio.

To investigate individual FLG flakes in terms of their area and NLs a high resolution 200-kV JEOL 2100F Field Emission Gun TEM

was used. Although more laborious, TEM analysis is a more accurate tool for lateral size, area and thickness estimation, as compared to AFM or dynamic light scattering [35]. One of the TEM investigated FLG flakes is shown at low magnification in Fig. 1b, while single layer graphene (SLG) fragment is shown in the high resolution TEM image in the inset. Another 5Ls edge of the flake is shown in Fig. 1c. 32 to 45 representative flakes were investigated for each of the samples prepared in different ULPE conditions. Further image processing was performed with ImageJ software in order to estimate the surface area and thickness of each flake. Statistical analysis of the measurements was performed.

XPS spectroscopy was applied for verification of potential graphene oxide (GO) presence in as-prepared graphene-water solution. The as-obtained graphene solution was vacuum filtered using a 0.2  $\mu\text{m}$  pore PTFE membrane. The graphene was collected from the membrane, transferred onto a Si wafer, and dried in a vacuum oven at 40 °C for 10 h. XPS spectra of the dried graphene were acquired from three separate regions of the sample using a monochromatic X-ray source (Thermo Scientific™ K-Alpha™ XPS spectrometer).

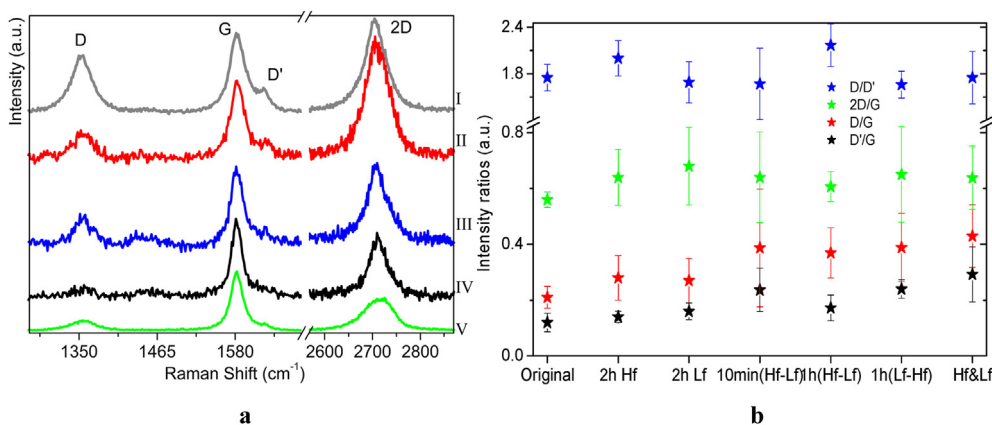


**Fig. 2.** Raman spectroscopy results. (a) Raman spectra diversity (I–IV spectra of 4 arbitrarily selected flakes), found in each US configuration, demonstrating the observed difference in intensity ratios between main Raman peaks. Spectrum V corresponds to the original GP. Spectral intensity is normalized to the intensity of the G peak, spectra are shifted along Y axis for clear observation. (b) Averaged intensity ratios of the main graphene related Raman peaks for different US set-ups, including data for the original graphite source GP and those published previously in Ref. [27] (2 h Lf and 2 h Hf). (A colour version of this figure can be viewed online.)

For all the studied samples a yield calculation was performed, following the procedure used and described in details previously [24,27]. It is based on the concentration ratio of the initial GP ( $C_0$ ) to the FLG flakes ( $C_G$ ),  $C_G/C_0$ . The final FLG flakes concentration  $C_G$  of the CF sample was estimated using the Lambert-Beer equation  $A = \alpha \times C_G \times l$  applied to the corresponding UV–vis spectra (see Section 3.1), where  $A$  is the absorption intensity at 660 nm,  $l$  is the cuvette path length [17,36]. The extinction coefficient  $\alpha$  was separately measured using the sample solution prepared in ULPE configuration called as “Hf&Lf together”. After centrifugation, one top part (2 ml) of the solution was collected for UV–vis measurement, another top part of the solution (100 ml) was vacuum filtered and dried in a vacuum overnight to determine the final concentration of the FLG flakes. UV–vis spectra were measured for 2 ml part of the CF sample diluted several times in DIW. Extinction coefficient was determined from the linear extrapolation of the plot for  $A/l$  at 660 nm vs  $C_G$ , described elsewhere [35]. The estimated value of the extinction coefficient was 1654 mL/(mg m).

### 3. Results and discussion

#### 3.1. Characterisation of the few-layer graphene

Quality of the FLG flakes obtained in different US set-up configurations was assessed by Raman spectroscopy and compared with the quality of the original GP samples and with the samples obtained previously [27] in single frequency ULPE set-ups. Examples of the typical Raman spectra obtained in this study and the Raman spectra of the original GP (spectrum V) are given in Fig. 2a. As-prepared FLG flakes demonstrated the spectra typical to  $sp^2$  hybridized carbon materials. They all contained clear graphene related peaks, among which the main Raman features were in-plane vibrational G mode around 1580  $cm^{-1}$ , two defect related bands around 1350 (D) and 1620  $cm^{-1}$  ( $D'$ ) and the 2nd order of Raman scattering so-called 2D band located around 2700  $cm^{-1}$  [37]. The obtained Raman spectra varied in terms of the intensity ratios between the main Raman peaks ( $D/D'$ ,  $D/G$  and  $2D/G$ ) even for the flakes of the same ULPE process. Spectra I and II in Fig. 2a with  $2D/G$  intensity ratio above one and with wide ( $\sim 60$   $cm^{-1}$ ) 2D band FWHM could be considered as the spectra from bilayer graphene [36], but spectrum I showed a higher defects level ( $D/G$  ratio is higher than 0.5 [36,37]). Although spectrum I showed a pronounced  $D'$  peak, which is related to the edge defects [37], the observed defectiveness was rather a sign of the small size of the investigated flake, than of the planar defects. That could be confirmed by the  $D/D'$  intensity ratio, which is in our case is below 3.5 [24]. Other two spectra (III and IV in Fig. 2a) were typical of FLG flakes with the  $2D/G$  intensity ratio around or smaller than one [27]. Some of the flakes demonstrated very low number of defects, which is observed from the spectrum like IV in Fig. 2a, where  $D/G$  intensity ratio is below 0.1 [24,27,36].

Fig. 2b shows the mean of different intensity ratio values. This plot contains not only data from combined sources (Hf and Lf) but also previously obtained data [27] from ULPE experiments where only one US source (Hf or Lf) was used as well as the Raman data for the original GP. The averaged data for presented intensity ratios look similar for all of the US configurations described here. The increasing  $2D/G$  intensity ratio compared to those of original GP indicate the thinning of the graphite, while the rising  $D/G$  intensity ratio points to the increased number of defects. Nevertheless, from the  $D/D'$  intensity ratio (blue stars trend) we can conclude that those defects mainly came from the edges, as the ratio is around 1.75, which is far below 3.5 according to Refs. [24,38,39]. The  $D/D'$  intensity ratio stayed within the same range as for the original graphite source and for the samples prepared by single-source

ULPE, while taking into account the statistical error. The ULPE with application of 2 US sources produced FLG flakes slightly more defective compared to the flakes that resulted from the single-US source ULPE (red and black stars trend). For the  $2D/G$  ratio (green stars) we did not see differences as compared to the previous results [27]. The  $2D/G$  intensity ratios were typical of FLG flakes [24,27,37]. Based on that we can conclude that during the ULPE processes studied here the thickness of exfoliated graphite flakes was reduced down to the thickness of FLG flakes, with some induced defects being mainly confined to the edge of FLG flakes.

The composition of the final CF solution was also verified by means of UV–vis spectroscopy as shown in Fig. 3. All spectra contained the peak around 270 nm, typical for the UV–vis spectra of graphene [27,33]. At the same time, we did not observe the GO related peak [34] around 230 nm for any of the as-prepared solutions. The absence of GO was further confirmed by XPS analysis that showed only the presence of graphene and some traces of Ti (apparently due to slight erosion of Ti sonotrode and membrane). The results are given in Supplementary Materials. The lowest absorbance intensity was detected for FLG solution (spectrum 4) prepared in US configuration “1 h/Hf–1 h/Lf”. For the ULPE in the reverse order (starting from Lf treatment), UV absorbance (spectrum 3) increased but remained still lower than the absorbance of the solutions obtained in the two other regimes (spectra 1 and 2). Based on this, we concluded that the sequential application of either Hf or Lf ULPE with a duration of 1 h each was not beneficial in terms of FLG concentration. It is worth noting that the lowest spectral intensity recorded for the sample prepared by regime “1 h/Hf–1 h/Lf” (spectrum 4) was still higher than the UV–vis absorbance intensity of the spectrum for the FLG flakes prepared by a single Hf US source reported previously [27] (indicated in Fig. 3 as “Hf only”). It was shown previously that the UV–vis absorbance intensity was proportional to the input power [27]. Given this, the concentration of the FLG flakes produced in the Hf ULPE set-up was limited by that parameter (higher power led to the solution overheating). The use of 2 US sources overcame that barrier (spectra 4 and 3). The intensities were higher than those of the spectrum obtained in a sole Hf set-up. Therefore, the application of the Lf sonotrode in combination with the Hf membrane helped to increase the FLG concentration, and in turn the yield. On the other hand, the application of Lf only gave the highest concentration when the other parameters remained similar (Fig. 3, upper spectrum indicated as “Lf only”). However, the quality of FLG flakes (in terms of size and thickness) was not good in this regime as will be demonstrated below by TEM results. In the case of two sources used, the solution with the highest concentration of FLG flakes was obtained in the ULPE, when both US sources simultaneously worked together for 2 h (spectrum 1). The spectral intensity registered for 2 US sources that alternated every 10 min (spectrum 2) were somewhat lower. Thus, the ULPE performed using 2 different-frequency US sources simultaneously provided the FLG flakes solution with a higher concentration, than that of the other studied combinations. This is further quantified by the yield estimates as shown in Table 1.

To the best of our knowledge the achieved here yield (10.5%) of FLG flakes with an average area of 1.5  $\mu m^2$  and the thickness of 3Ls is comparable to the best results for LPE produced graphene in water. Turner et al. presented even higher yield of 16% (Fig. 3a in Ref. [24]), for their LPE system but with sodium cholate as a surfactant. Moreover, their produced FLG flakes were of larger average thickness (5–6 Ls), and much smaller average area ( $\sim 0.015$   $\mu m^2$  in Ref. [24]). A higher yield of 12.5% was reported in our previous work on water based ULPE for a single Lf sonotrode configuration [27], but that was achieved at a higher US power. In the dual frequency configuration described here the power for both of the US sources



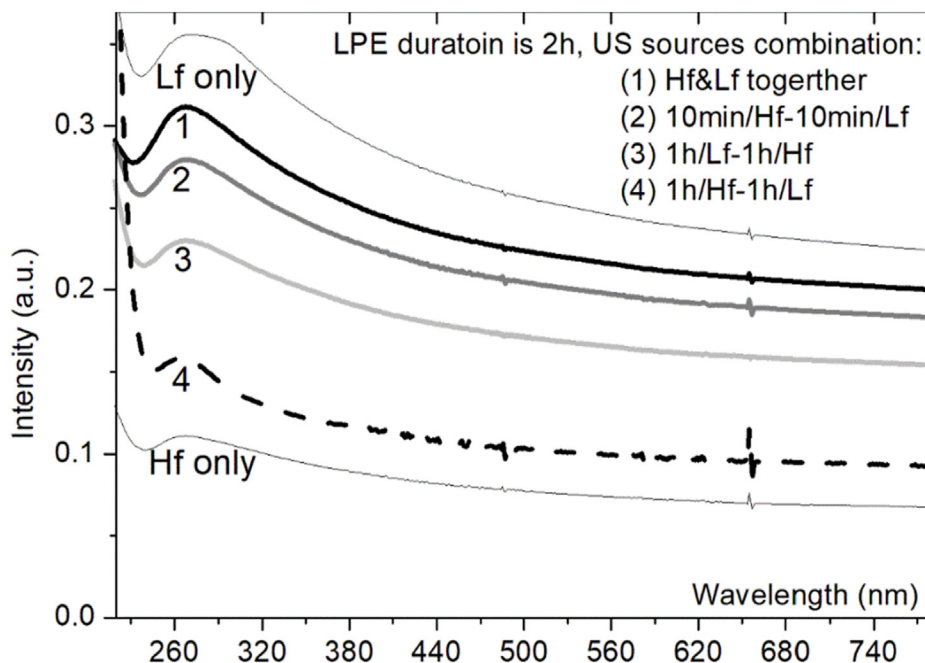


**Fig. 3.** UV–vis spectra for the samples obtained at 6 different regimes of exfoliation process. Corresponding configuration parameters (time/US source type) are indicated in the graph legend by number for each UV–vis spectrum. UV–vis spectra of the solution obtained with only one type of source are shown by thin grey lines (after [27]) and marked correspondingly as “Lf only” or “Hf only”.

**Table 1**

Estimated yield of exfoliation for the ULPE configurations shown in Fig. 3.

ULPE configuration	Yield (%)
Lf	10.5
Hf&Lf together	9.7
10min/Hf–10min/Lf	9
1 h/Lf–1 h/Hf	8.7
1 h/Hf–1 h/Lf	7.7
Hf	4.8

was kept at 50% to avoid the overheating of the solution. Other reports on the LPE in water [25,28] gave the yield below 7%, but for much smaller flakes.

The yield is a significant parameter of the process, but the quality of the FLG materials is even more important. To get more information on the quality of as-prepared FLG flakes, i.e., thickness and size, TEM investigation was performed. Randomly chosen 32–45 flakes were analysed on a TEM grid for each ULPE regime to identify their area and thickness, using low and high resolution TEM mode, respectively. Fig. 4a gives the summary of the TEM investigation presented as the size and area distribution not only for FLG flakes prepared in this work by combined regimes, but also for the flakes prepared using a single source in our previous studies [27] and for the commercially available graphene as a benchmark. Fig. 4b shows the average values with the error bars of the data in Fig. 4a.

As one can see, except for the configuration “1 h/Hf–1 h/Lf” where the average thickness was about 10 Ls and the area around  $1 \mu\text{m}^2$  (open squares in Fig. 4), the average thickness of as-obtained FLG flakes (corresponding data are shown by star, triangular and cross symbols in Fig. 2b) was significantly reduced down to 5 Ls or less and the mean area was enlarged up to 2 and more  $\mu\text{m}^2$  compared to the samples prepared during the same US treatment time by only one of the mentioned US source (open and black hexagons symbols). Given that the sample “1 h/Hf–1 h/Lf” also

demonstrates a low concentration of the solution (Fig. 3, spectrum 4), we can conclude that the efficiency of the Hf source is not enough to initiate exfoliation and disperse the thinning GP particles in the 1st h of ULPE. As a result, after the 1st h of ULPE significant part of graphite particles sedimented due to their bulky mass and due to the weak US-induced mixing flow. It was shown previously in Ref. [27] that the cavitation intensity of Hf set-up was much lower compared to Lf US process of the same input power. That was also observed visually, when initially black solution of just added GP became slightly transparent after 1 h of ULPE, and at the end of the process GP particles were found at the bottom of the beaker around the membrane.

The hypothesis of the weak dispersive capability of Hf set-up was confirmed by the additional ULPE process with the inverse order of the applied US sources. Solution obtained in the ULPE configuration “1 h/Lf – 1 h/Hf”, when Lf sonotrode was applied for the 1st h of treatment, showed the UV–vis spectrum of a significantly higher absorbance (Fig. 3, spectrum 3), and hence, higher concentration. During this process the acoustic streaming induced by the Lf field dispersed the GP in the DIW and the active cavitation bubbles reduced their size and thickness during the 1st h so that the suspension became more stable. After that, the acoustic streaming of the Hf US field was enough to further and more effectively exfoliate the suspended particles down to 5 Ls in average, as shown in Fig. 4 by the crosses. Hence, a right combination of 2 US sources increased the size and reduced the thickness of the FLG flakes as compared to any of the single sources (at the same input power). The best results in terms of the thickness and area were obtained for FLG flakes produced by ULPE process when both the Lf and Hf were applied simultaneously for 2 h (black stars in Fig. 4): FLG average thickness is 3 Ls with the area of  $1.5 \mu\text{m}^2$ . Note that although this thickness was close to the thickness of commercially produced graphene “Eau de Graphene” (black dot in Fig. 2b), the average area in our case was 3 times larger.

In our previous paper [27] we suggested that Lf cavitation produced larger bubbles (up to few hundreds of micron size) that emit

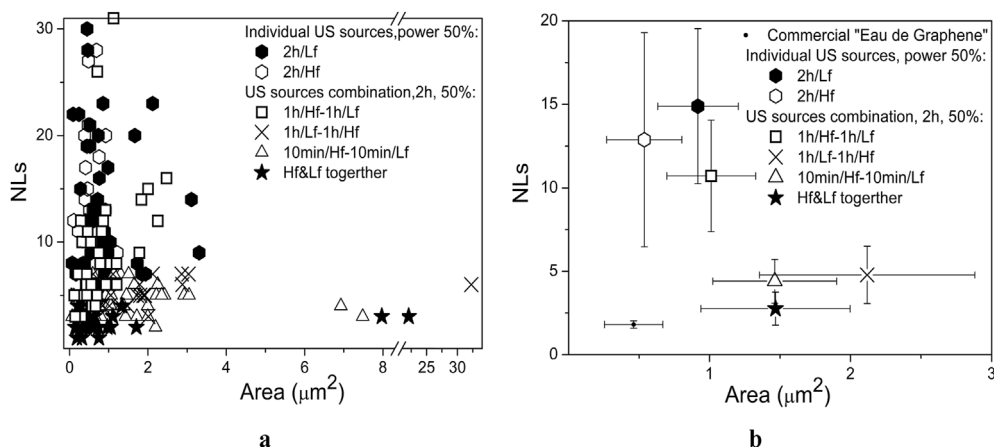


**Fig. 4.** (a) TEM data presented as the surface area and NLS distribution for each examined flake in dependence on the ULPE configuration. Corresponding configuration parameters (time/US source type) are indicated in the graph legend by symbols. Data for individual US sources from previously published results [27] are shown for comparison, marked by black and open hexagons. (b) The average data of the main TEM plot in (a). Additional data for commercially produced graphene (Eau de Graphene) is shown for comparison in (b).

stronger shock waves (SWs) upon their implosion, while Hf cavitation generated much smaller bubbles (in the range of a few microns) that oscillate in a more stable manner with milder emissions. Therefore, it was hypothesized that the Lf processing played a major role in the initial splitting of graphite plates while Hf treatment offered a “gentler” exfoliation of graphite by working between preliminary split and expanded graphite layers. Recently, our group revealed a number of manifestations of ULPE of graphite in water that directly confirmed these mechanisms, albeit without changing the frequency of the processing [40]. It has been experimentally demonstrated that larger cavitation bubbles expand the graphite flakes upon implosion due to strong SWs emissions, split the flakes due to micro-liquid jet interactions and pull the interlayers apart by large oscillations, while smaller bubbles (also generated by the implosion of the larger ones) penetrate between the split layers to facilitate further exfoliation via expansion [39]. Hence, the combination of these two cavitation regimes should be beneficial for the quality and quantity of the exfoliated graphene, as has been demonstrated in this Section. In order to further study the characteristics of the Lf and Hf ULPE processing we measured the acoustic emissions/acoustic pressure for a number of the studied regimes.

### 3.2. Acoustic pressure measurements

The driving force for ULPE is cavitation that can be characterised by acoustic emissions. In the previous paper [27] we measured the overall intensity of broadband noise, measured in terms of electrical output (mV), to compare various regimes of ULPE. Acoustic pressure (in Pa), both maximum and root-mean-square (RMS), is, however, a better measure of ultrasonic cavitation environment as it provides physical, and consequently practical, meaning to cavitation measurements within the studied solutions. Therefore, in this study we measured acoustic spectra and pressure using two cavitation acoustic sensors calibrated for low and high frequency ranges, needle hydrophone (NH) and fiber-optic hydrophone (FOH), respectively able to capturing the acoustic emissions from both transducers (from kHz up to MHz range). Acoustic pressure spectra were detected for 3 US configurations (Hf, Lf and Hf&Lf) in DIW: before ULPE, just after adding the GP (ULPE start) and every hour till the end of ULPE process. The results of acoustic pressure measurements are summarised in Table 2.

First thing to note is that for all settings the acoustic pressures increase after adding the GP into the DIW (see the bold numbers in

Table 2 reflecting the measurements adequate to the source driving frequency, for DIW and DIW + GP/0 h). Such an increase in the pressure is rather logical as graphite/water interfaces would be expected to increase the number density of nucleation sites for cavitation bubbles. The addition of flakes, therefore, promoted stronger acoustic emissions because they became favourable sources of bubbles formation or attracted collapsing events (facilitated by the initially hydrophobic nature of graphite [41,42]), significantly amplifying the cavitation occurrence and possibly the exfoliation process. The acoustic pressure measured in the MHz range reflected both the cavitation caused by the Hf source and the acoustic emissions (SWs) from imploding bubbles formed by the Lf source [43]. By increasing the time of ULPE the acoustic emissions in the MHz range (captured by FOH) decreased, which reflected the formation of hydrophilic graphene that did not have the same enhancing effect on cavitation nucleation as hydrophobic graphite (Table 2, the data for FOH). In all stages of the LPE process, the cumulative pressure achieved by two US sources was higher than the sum of pressures from the two individual sources measured by the sensors, which were calibrated for relevant frequency ranges (Table 2, shown in bold letters):  $NH(Lf) + FOH(Hf) < NH + FOH(Lf \& Hf)$ . This is in agreement with the effect of cavitation enhancement upon using different-frequency sources described in Ref. [44].

Fig. 5 shows a number of typical spectra for different US set-ups taken in the mid-stage (after 50 min) of the ULPE. The original broadband signal that contains all the low- and high-frequency linear and non-linear components from the acoustic source and the cavitating bubbles exhibits 7 times higher amplitudes in the kHz range as seen by the insets of Fig. 5a and b. This is expected as the larger bubbles formed by the Lf source are prone to vigorous oscillations and repetitive collapses as compared to the tiny (a few microns size) stable Hf bubbles, generating powerful emissions and thus raising the amplitude of the cavitation spectrum [45]. The spectra captured by both sensors contain typical acoustic features in terms of expected frequencies. Strong peaks corresponding to the driving frequencies of the US sources are visible at 1174 kHz (FOH) and at 24 kHz (NH). The FOH is not calibrated for the Lf range, so there is no peak captured around 24 kHz. Similarly, the NH is not calibrated for emissions above 400 kHz and, hence, there is no driving frequency of the Hf source. The spectra also show the corresponding ultra- and sub-harmonic emission peaks.

The FOH spectra are characterised by a well-pronounced broad peak at about 3.45 MHz, which can be clearly seen in Fig. 5a, c.

**Table 2**

Variation of the RMS acoustic pressure (by FOH/NH<sup>a</sup>) in dependence on the ULPE stage and configuration. Data from the sensors calibrated for relevant frequency ranges are shown in bold.

LPE stages	Lf (kPa)		Hf (kPa)		Lf&Hf (kPa)	
	FOH	NH	FOH	NH	FOH	NH
DIW	41 ± 2.1	<b>43 ± 7</b>	<b>46 ± 23</b>	5.1 ± 0.6	<b>81 ± 4</b>	<b>32 ± 2.1</b>
DIW + GP/0 h	18 ± 1.5	<b>97 ± 12</b>	<b>77 ± 22</b>	6 ± 0.17	<b>57 ± 15</b>	<b>148 ± 2.8</b>
DIW + GP/1 h	17 ± 6.2	<b>105 ± 41</b>	<b>38 ± 23</b>	9 ± 7.7	<b>31 ± 8.5</b>	<b>145 ± 66</b>
DIW + GP/2 h	21 ± 0.25	<b>125 ± 5</b>	<b>14 ± 2.3</b>	3.5 ± 2	<b>25 ± 1.2</b>	<b>130 ± 6</b>

<sup>a</sup> NH is calibrated in the range up to 400 kHz and characterizes mostly emissions from the Lf source; while FOH is calibrated from 1 to 30 MHz and characterizes mostly emissions from the Hf source as well as high-frequency emission from cavitating bubbles including shock waves. These pressure measurements are on top of the atmospheric pressure (as sensors were calibrated at atmospheric pressures).

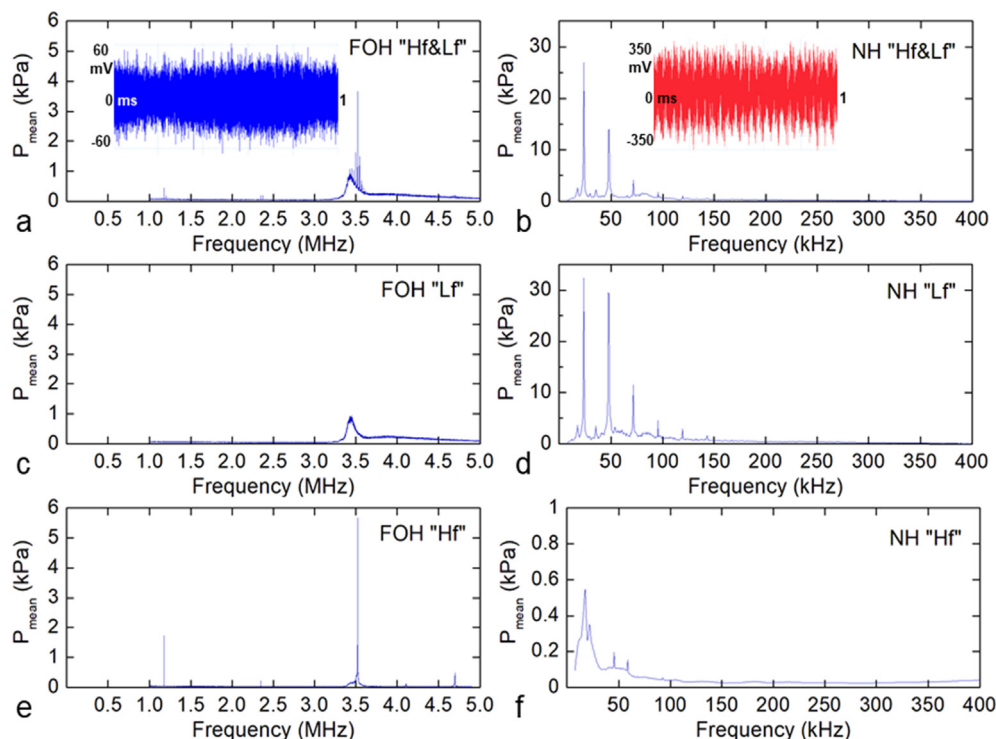


**Fig. 5.** Examples of spectral acoustic measurements at the middle stage of the ULPE process (50 min) in different configurations (a, b) "Hf&Lf together", (c, d) just Lf and (e, f) just Hf: (a, c, e) spectra obtained using the FOH sensor sensitive only to high-frequency emissions; (b, d, f) spectra registered by the NH sensor sensitive only to lower frequency emissions. Corresponding waveforms for the general noise intensity for "Hf&Lf together" set-up are shown in insets (a, b). Based on such data, the maximum and RMS acoustic pressures were estimated (see Table 2 and text). Note different Y-axis scales. (A colour version of this figure can be viewed online.)

According to Ref. [30] it corresponds to the SW emissions by imploding cavitation bubbles and plays a decisive role in the exfoliation process [39]. Note that for the Lf set-up (Fig. 5c) this peak looks broader when the Lf source is working in addition to the Hf membrane (Fig. 5a), reflecting a wider size range of active bubbles. In the absence of Lf source, the SW peak in Fig. 5e is about 3 times smaller in intensity probably due to the fact that smaller bubbles produced by Hf-generate lesser pressure upon collapse as compared to larger bubbles associated with Lf cavitation. Another observation relates to the 3rd Hf harmonic, which appear to be within the area of SW peak at 3.52 MHz as a single very sharp peak for Hf set-up. Its intensity is at least 3 times higher than the 1st harmonic (Fig. 5e). Its appearance may be due to the bubbles related to the harmonic cascading as explained in Ref. [46]. Also, it could be the effect of non-linearity parameter of the host medium due to the introduction of graphite powder that promotes waveform distortions that coincide with the raise of this peak. Interestingly, when these 2 sources are combined the 1st and 3rd harmonics are still present though suppressed by about 1.5 times

(Fig. 5a). The 3rd harmonic still remains several times higher than its 1st harmonic at 1174 kHz. In addition, many prominent sharp peaks emerged around 3rd harmonic on top of the broad SW peak indicating a constant vibrating regime from vigorously resonating bubbles (in the range of 0.8  $\mu\text{m}$ , about 3 times less of the initial bubble size at 1174 kHz) as shown in Ref. [31], which might have been triggered by the SWs emissions [42].

On the other hand, the NH did not show significant response for the Hf source as it was not sensitive to the high-frequency emissions. Some unexpected low intensity peaks visible in Fig. 5f in the range of 0–100 kHz may be related with standing waves due to the size of the container (reflections from the free surface and the walls). For the other 2 cases of Lf (Fig. 5d) and Lf&Hf (Fig. 5b) the spectra capture by the NH did not show any significant features apart from harmonics of the driving frequency (including the rise of a sub-harmonic peak at 48, 72 and 96 kHz that is an indication of the established cavitation regime). The suppression of the second and third harmonic in the combined regime (Fig. 5b) by 50% and 70%, respectively, may be an indication of absorbing the acoustic

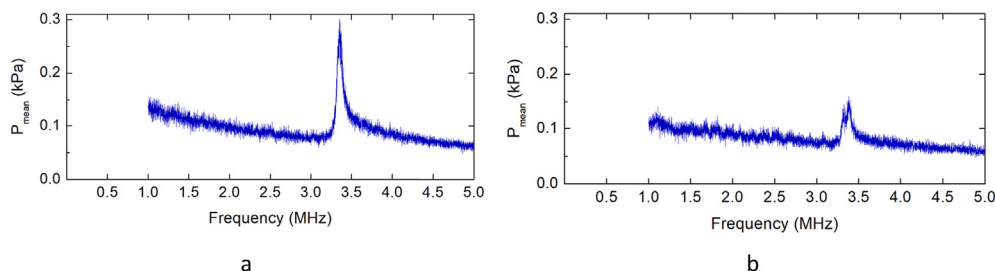


**Fig. 6.** Acoustic spectra of the Lf set-up registered by FOH: (a) in DIW and (b) after GP was added. (A colour version of this figure can be viewed online.)

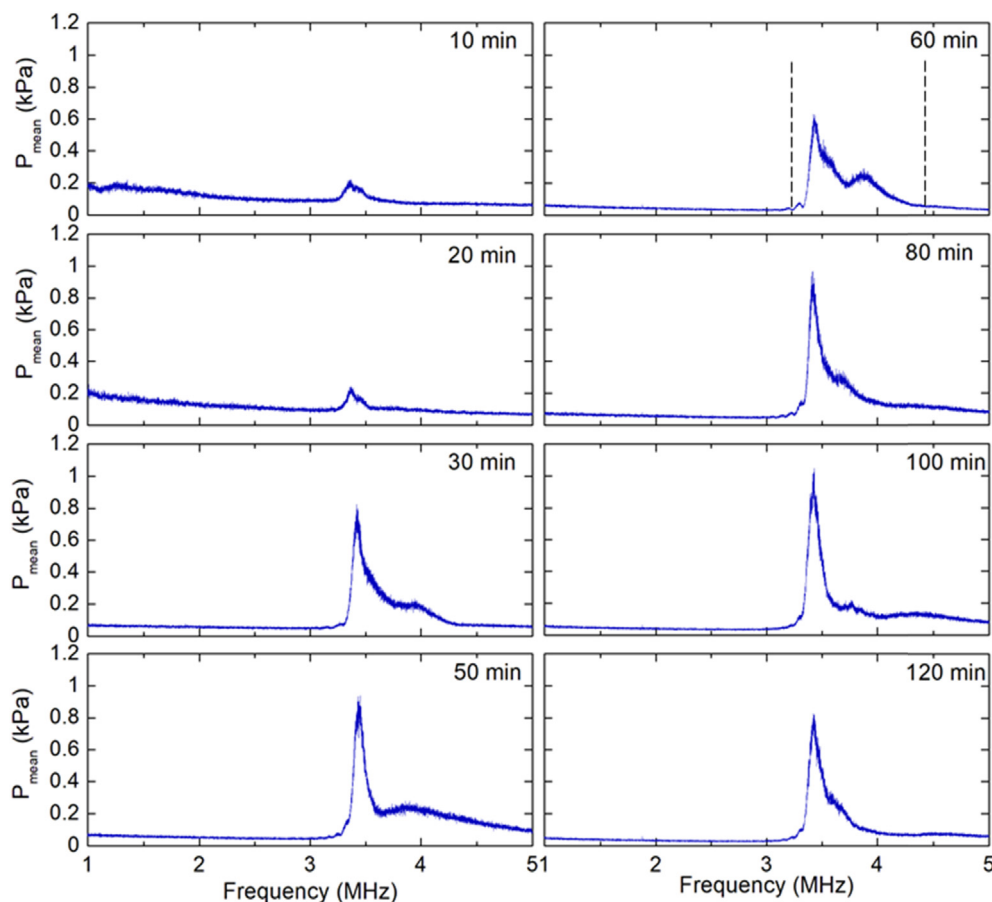


**Fig. 7.** Evolution of the SWs peak shape throughout the ULPE of GP in DIW by Lf only. FOH acoustic spectra were registered at different moments of time (noticed below each spectrum). Dashed lines for 60 min spectrum indicate the analysed peak base width. (A colour version of this figure can be viewed online.)

energy by 1) numerous tiny oscillating bubbles generated by the Hf source that are manifested as prominent peaks at higher frequencies (as discussed above) or 2) large oscillating bubbles that after implosion transferred part of their energy via SWs to higher frequencies (Fig. 5a). It is clear that the lower-frequency emissions captured by the NH reflect the high acoustic pressure generated by the overall cavitation when the Lf source is involved (Fig. 5b, d).

There are few phenomena that may have happened in this dual-frequency approach: 1) implosions of the bubbles appeared under the Lf US field create cavitation fragments (satellite bubbles) that may become active bubbles in the Hf US field; 2) a combined frequency sound field is formed due to nonlinear interaction of sound waves [43,47], which excites cavitation over a wider range of cavitation bubble radii than any single-frequency sonication; 3) the mass transfer through acoustic streaming is more efficient when

two US sources are acting and generating streaming in opposite directions, from the top (Lf) and bottom (Hf), which not only increases the active cavitation zone but also treatment efficiency; 4) microbubbles in the range of a few microns generated by the Hf source and fragments of collapsed larger bubbles from the Lf source are expected to dominate the solution promoting a gentler exfoliation as previously shown in Refs. [27,39]. A combination of these phenomena explains the improved quality at a high yield of ULPE when using dual-frequency settings. With regard to the slightly increased number of the defects of the FLG flakes processed in dual frequency regime (observed by Raman spectroscopy, Fig. 2b), we need to take into account not only the RMS but peak values of the pressure. The highest pressure for Lf ULPE registered by the NH was  $390 \pm 54$  kPa, for Hf registered by the FOH was  $60 \pm 7$  kPa, while for the Lf&Hf configuration it was  $120 \pm 7$  kPa registered by the FOH,



and  $405 \pm 33$  kPa registered by the NH. The higher the value of this peak pressure emission, the more likely mechanical damage may occur to the flakes being processed in due time.

Having identified the presence of SWs (Fig. 5a, c) and knowing that these SWs are instrumental in exfoliation [39], next step was to check the evolution of the SW broad peak at 3.2–3.5 MHz as an indicator on the exfoliation process of graphite upon ULPE. For this set of experiments, only the Hf sensor able to resolve SW emissions was deployed. Fig. 6 shows that the SWs peak intensity of the DIW spectrum was almost twice as compared to that of GP-water solution at the start of ULPE. That could be explained by the fact that added GP particles obstructed the SWs propagation in the DIW due to their interaction with graphite: SWs energy dissipated or was absorbed by bulk graphite as the result of the GP particles exfoliation. After adding GP, the SWs peak not only reduced in intensity but also developed more complex shape via splitting (Fig. 6).

Throughout the LPE process the shape evolution continued, and wider shoulders to the main peak around 3.45 MHz appeared and changed their position, width and intensity, as shown in Fig. 7. After 30 min of ULPE process the SWs peak intensity became higher than that of DIW spectrum (compare Figs. 7 and 6a), which may be indicative of the advanced stage of exfoliation. The additional peaks could be explained by the varying nature of the solution after GP is added and treated for some time: GP particles break apart into smaller and thinner pieces, their interaction with SWs becomes more complex. We can suggest (though this requires further investigation) that the absorbance coefficient of SWs in FLG flakes at MHz depends on their thickness: thinner flakes allow SWs to propagate in the liquid and reach the probe, raising the amplitude and forming a sharper less distorted single peak. As one can see in Fig. 7 that happened after 100 min of LPE, probably meaning that the solution became more uniform in terms of the FLG flakes thickness.

Further analysis of the width at the base of SW peak (shown in Fig. 7 for spectrum after 60 min of UPLE treatment) vs ULPE duration time have shown that the widest SWs peak is appeared after 50 min of the exfoliation process. The resulting plot is given in Fig. 8. After 50–60 min, the width of the peak base decreases and stabilises for the last 20–30 min of ULPE, remaining still wider than the width of the SWs peak at pure water. We interpret these observations that in the period from 20 to 50 min, GP intensively split apart and exfoliate to thinner species. According to our hypothesis the variety of the flake sizes and thicknesses gives rise to a larger width of the SWs peak. At 50 min the GP–DIW mixture is the most nonuniform in terms of the flake size and thickness distribution. In summary, one would expect a thinner and sharper peak (resembling to that of the DIW in Fig. 6a) when the more homogeneous

mixture with graphene flakes is achieved. In our experiment (Fig. 8) the peak width stabilises after 100 min of the LPE process, reaching the more homogeneous environment with mostly FLG flakes.

As-observed phenomenon and our hypothesis open up the route to monitor in-situ the stages of the LPE process (at the moment in terms of the flake thickness uniformity) for FLG production. To the best of our knowledge this kind of opportunity was not reported before. Further step-by-step investigation of the DIW–GP mixture composition through the time is needed to verify the identified change in the SW peak shape.

#### 4. Conclusion

We demonstrate a novel method for ULPE of graphite to produce high quality and relatively large in size graphene of up to 3-layers thickness in a benign environment in just 2-h. A systematic study of dual ultrasonic frequency (24 kHz + 1174 kHz) ULPE process configurations was performed with the assessment of the FLG flakes quality, ULPE yield and acoustic characteristics. The ULPE set-ups varied by changing the order of the applied US fields created by Lf and Hf sources. Complex characterisation of the as-obtained FLG flakes, including UV–vis, Raman, XPS spectroscopies and TEM analysis, showed that the 2 h ULPE process performed simultaneously by Lf and Hf US sources reduced the average thickness of the FLG flakes down to 3 layers keeping their average area around  $1.5 \mu\text{m}^2$ . According to the UV–vis investigation this kind of combination of the US sources provided the highest concentration of the flakes compared to other tested set-ups with alternating order of the sources, with the yield approaching 10%. The acoustic characterisation of the ULPE process demonstrated a synergetic effect of two US sources of different frequencies on the acoustic pressure generated in the processed volume, as well as the effect of graphite particles and formed graphene under controlled acoustic pressure conditions. The acoustic spectra obtained in different frequency ranges revealed the presence of SW emissions. It is suggested that the width of the SW emission peak can be used for in-situ monitoring of ULPE process. Further studies will be focused on the effects of the initial graphite dimensions and quality on the graphene production parameters as well as on studying the functional properties of the produced graphene sheets.

#### CRediT authorship contribution statement

**Anastasia V. Tyurnina:** Conceptualization, Data curation, Methodology, Formal analysis, Investigation, Validation, Visualization, Writing – original draft. **Justin A. Morton:** Investigation, Data curation, Methodology, Visualization, Writing – review & editing. **Tungky Subroto:** Investigation, Methodology, Writing – review & editing. **Mohammad Khavari:** Visualization, Writing – review & editing. **Barbara Maciejewska:** Investigation. **Jiawei Mi:** Funding acquisition. **Nicole Grobert:** Resources, Funding acquisition. **Kyriakos Porfyrakis:** Funding acquisition. **Iakovos Tzanakis:** Conceptualization, Funding acquisition, Methodology, Resources, Writing – review & editing. **Dmitry G. Eskin:** Conceptualization, Methodology, Funding acquisition, Project administration, Resources, Supervision, Writing – review & editing.

#### Declaration of competing interest

The authors declare that they have no known competing financial interests or personal relationships that could have appeared to influence the work reported in this paper.

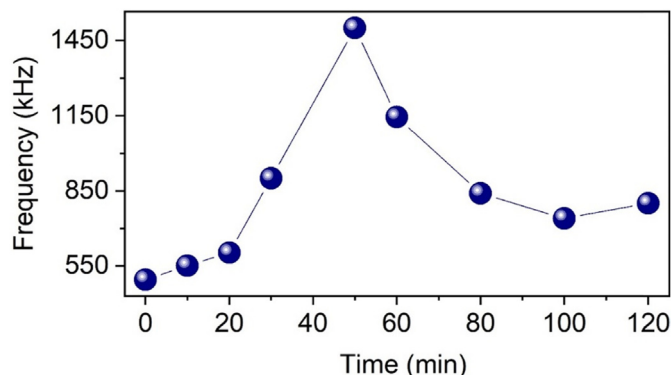


Fig. 8. Evolution of the SWs peak base width throughout the ULPE of GP in DIW by Lf only. (A colour version of this figure can be viewed online.)

## Acknowledgments

This study is a part of the project “Sustainable and industrially scalable ultrasonic liquid phase exfoliation technologies for manufacturing 2D advanced functional materials” (EcoUltra2D) funded by the UK Engineering and Physical Sciences Research Council (EPSRC) under the grant nos. EP/R031665/1; EP/R031401/1; EP/R031819/1; EP/R031975/1.

## Appendix A. Supplementary data

Supplementary data to this article can be found online at <https://doi.org/10.1016/j.carbon.2021.09.036>.

## References

- [1] K.S. Novoselov, A.K. Geim, S.V. Morozov, D. Jiang, Y. Zhang, S.V. Dubonos, et al., Electric field effect in atomically thin carbon films, *Science* 306 (2004) 666–669, <https://doi.org/10.1126/science.1102896>.
- [2] A.A. Balandin, S. Ghosh, W. Bao, I. Calizo, D. Teweldebrhan, F. Miao, C.N. Lau, Superior thermal conductivity of single-layer graphene, *Nano Lett.* 8 (3) (2008) 902–907, <https://doi.org/10.1021/nl0731872>.
- [3] R.R. Nair, P. Blake, A.N. Grigorenko, K.S. Novoselov, T.J. Booth, T. Stauber, N.M.R. Peres, A.K. Geim, Fine structure constant defines visual transparency of graphene, *Science* 320 (5881) (2008) 1308, <https://doi.org/10.1126/science.1156965>, 1308.
- [4] K.S. Novoselov, V.I. Fal'ko, L. Colombo, P.R. Gellert, M.G. Schwab, K. Kim, A roadmap for graphene, *Nature* 490 (7419) (2012) 192–200, <https://doi.org/10.1038/nature11458>.
- [5] M.M. Tavakoli, R. Tavakoli, P. Yadav, J. Kong, Graphene/ZnO electron transfer layer together with perovskite passivation enable highly efficient and stable perovskite solar cells, *J. Mater. Chem., A* 7 (2019) 679–686, <https://doi.org/10.1039/c8ta10857a>.
- [6] E. Gibney, Surprise graphene discovery could unlock secrets of superconductivity, *Nature* 555 (7695) (2018) 151–152, <https://doi.org/10.1038/d41586-018-02773-w>.
- [7] A. Bylinkin, E. Titova, V. Mikheev, E. Zhukova, S. Zhukov, M. Belyanchikov, M. Kashchenko, A. Miakonikh, D. Svintsov, Tight-binding terahertz plasmons in chemical-vapor-deposited graphene, *Phys. Rev. Appl.* 11 (5) (2019), 054017, <https://doi.org/10.1103/PhysRevApplied.11.054017>, 8.
- [8] H. Jang, Z. Dai, K.H. Ha, S.K. Ameri, N. Lu, Stretchability of PMMA-supported CVD graphene and of its electrical contacts, *2D Mater.* 7 (1) (2020), 014003, <https://doi.org/10.1088/2053-1583/ab4c0f>, 29.
- [9] Ö. Kutun, E. Öztumur, A. Sadler, 60 Uses of graphene – the ultimate guide to graphene's (potential) applications in. <https://nanografi.com/blog/60-uses-of-graphene/>, 2019. (Accessed July 2018) accessed.
- [10] S. Park, R.S. Ruoff, Chemical methods for the production of graphenes, *Nat. Nanotechnol.* 4 (2009) 217–224, <https://doi.org/10.1038/nnano.2009.58>.
- [11] K.R. Paton, E.V. Varria, C. Backes, R.J. Smith, U. Khan, J.N. Coleman, et al., Scalable production of large quantities of defect-free few-layer graphene by shear exfoliation in liquids, *Nat. Mater.* 13 (2014) 624–630, <https://doi.org/10.1038/nmat3944>.
- [12] W. Kong, H. Kum, S.H. Bae, J. Shim, H. Kim, L. Kong, et al., Path towards graphene commercialization from lab to market, *Nat. Nanotechnol.* 14 (2019) 927–938, <https://doi.org/10.1038/s41565-019-0555-2>.
- [13] S. Gravelle, C. Kamal, L. Botto, Liquid exfoliation of multilayer graphene in sheared solvents: a molecular dynamics investigation, *J. Chem. Phys.* 152 (8) (2020) 104701, <https://doi.org/10.1063/1.5141515>.
- [14] Y. Xu, H. Cao, Y. Xue, B. Li, W. Cai, Liquid-phase exfoliation of graphene: an overview on exfoliation media, techniques, and challenges, *Nanomaterials* 8 (11) (2018) 942, <https://doi.org/10.3390/nano8110942>, 1–32.
- [15] H. Tao, Y. Zhang, Y. Gao, Z. Sun, C. Yan, J. Texter, Scalable exfoliation and dispersion of two-dimensional materials – an update, *Phys. Chem. Chem. Phys.* 19 (2) (2017) 921–960, <https://doi.org/10.1039/c6cp06813h>.
- [16] A. Ciesielski, P. Samorì, Graphene via sonication assisted liquid-phase exfoliation, *Chem. Soc. Rev.* 43 (2014) 381–398, <https://doi.org/10.1039/C3CS60217F>.
- [17] M. Lotya, P.J. King, U. Khan, S. De, J.N. Coleman, High-concentration, surfactant-stabilized graphene dispersions, *Nano* 4 (6) (2010) 3155–3162, <https://doi.org/10.1021/nl1005304>.
- [18] C.E. Hamilton, J.R. Lomeda, Z. Sun, J.M. Tour, A.R. Barron, High-yield organic dispersions of unfunctionalized graphene, *Nano Lett.* 9 (10) (2009) 3460–3462, <https://doi.org/10.1021/nl9016623>.
- [19] S. Haar, M. El Gemayel, Y. Shin, G. Melinte, M.A. Squillaci, O. Ersen, C. Casiraghi, A. Ciesielski, P. Samorì, Enhancing the liquid-phase exfoliation of graphene in organic solvents upon addition of n-octylbenzene, *Sci. Rep.* 5 (1) (2015) 16684, <https://doi.org/10.1038/srep16684>, 9.
- [20] R. Narayan, S.O. Kim, Surfactant mediated liquid phase exfoliation of graphene, *Nano Convergence* 2 (1) (2015) 20, <https://doi.org/10.1186/s40580-015-0050-x>, 19.
- [21] J.N. Coleman, Liquid exfoliation of defect-free graphene, *Acc. Chem. Res.* 46 (1) (2013) 14–22, <https://doi.org/10.1021/ar300009f>.
- [22] L. Lin, H. Peng, Z. Liu, Synthesis challenges for graphene industry, *Nat. Mater.* 18 (2019) 520–524, <https://doi.org/10.1038/s41563-019-0341-4>.
- [23] M. Yi, Z. Shen, S. Liang, L. Liu, X. Zhang, S. Ma, Water can stably disperse liquid-exfoliated graphene, *Chem. Commun.* 49 (2013) 11059–11061, <https://doi.org/10.1039/c3cc46457a>.
- [24] P. Turner, M. Hodnett, R. Doray, J.D. Carey, Controlled sonication as a route to in-situ graphene flake size control, *Sci. Rep.* 9 (8) (2019) 8710, <https://doi.org/10.1038/s41598-019-45059-5>.
- [25] K.B. Ricardo, A. Sendecki, H. Liu, Surfactant-free exfoliation of graphite in aqueous solutions, *Chem. Commun. (J. Chem. Soc. Sect. D)* 50 (2014) 2751–2754, <https://doi.org/10.1039/C3CC49273G>.
- [26] V. Chabot, B. Kim, B. Sloper, C. Tzoganakis, A. Yu, High yield production and purification of few layer graphene by Gum Arabic assisted physical sonication, *Sci. Rep.* 3 (7) (2013) 1378, <https://doi.org/10.1038/srep01378>.
- [27] A.V. Tyurnina, I. Tzanakis, J. Morton, J. Mi, K. Porfyrakis, D.G. Eskin, et al., Ultrasonic exfoliation of graphene in water: a key parameter study, *Carbon* 168 (2020) 737–747, <https://doi.org/10.1016/j.carbon.2020.06.029>.
- [28] J. Kim, S. Kwon, D.H. Cho, B. Kang, H. Kwon, Y. Kim, et al., Direct exfoliation and dispersion of two-dimensional materials in pure water via temperature control, *Nat. Commun.* 6 (9) (2015) 8294, <https://doi.org/10.1038/ncomms9294>.
- [29] L.A. Belyaeva, P.M.G. Deursen, K.I. Barbetse, G.F. Schneider, Hydrophilicity of graphene in water through transparency to polar and dispersive interactions, *Adv. Mater.* 30 (7) (2018) 1703274, <https://doi.org/10.1002/adma.201703274>.
- [30] M. Khavari, A. Priyadarshi, A. Hurrell, K. Pericleous, D. Eskin, I. Tzanakis, Characterization of shock waves in power ultrasound, *J. Fluid Mech.* (14) (2021) 915, <https://doi.org/10.1017/jfm.2021.186>, R3.
- [31] I. Tzanakis, G.S.B. Lebon, D.G. Eskin, K.A. Pericleous, Characterizing the cavitation development and acoustic spectrum in various liquids, *Ultrason. Sonochem.* 34 (2017) 651–662, <https://doi.org/10.1016/j.ultrasonch.2016.06.034>.
- [32] A.M. Hurrell, S. Rajagopal, The practicalities of obtaining and using hydrophone calibration data to derive pressure waveforms, *IEEE Trans. Ultrason. Ferroelectrics Freq. Contr.* 64 (1) (2017) 126–140, <https://doi.org/10.1109/TUFFC.2016.2594770>.
- [33] V.G. Kravets, A.N. Grigorenko, R.R. Nair, P. Blake, S. Anisimova, K.S. Novoselov, et al., Spectroscopic ellipsometry of graphene and an exciton-shifted van Hove peak in absorption, *Phys. Rev. B* 81 (15) (2010) 155413, <https://doi.org/10.1103/PhysRevB.81.155413>, 14.
- [34] Q. Lai, S. Zhu, X. Luo, M. Zou, S. Huang, Ultraviolet-visible spectroscopy of graphene oxides, *Appl. Phys. Lett.* 101 (2012), 032146, <https://doi.org/10.1063/1.4747817>.
- [35] M. Lotya, A. Rakovich, J.F. Donegan, J.N. Coleman, Measuring the lateral size of liquid-exfoliated nanosheets with dynamic light scattering, *Nanotechnology* 24 (7) (2013) 265703, <https://doi.org/10.1088/0957-4484/24/7/265703>.
- [36] M. Lotya, Y. Hernandez, P.J. King, R.J. Smith, et al., Liquid phase production of graphene by exfoliation of graphite in surfactant/water solutions, *J. Am. Chem. Soc.* 131 (10) (2009) 3611–3620, <https://doi.org/10.1021/ja807449u>.
- [37] A.C. Ferrari, Raman spectroscopy of graphene and graphite: disorder, electron–phonon coupling, doping and nonadiabatic effects, *Solid State Commun.* 143 (2007) 47–57, <https://doi.org/10.1016/j.ssc.2007.03.052>.
- [38] A. Eckmann, A. Felten, A. Mishchenko, L. Britnell, R. Krupke, K.S. Novoselov, et al., Probing the nature of defects in graphene by Raman spectroscopy, *Nano Lett.* 12 (8) (2012) 3925–3930, <https://doi.org/10.1021/nl300901a>.
- [39] C. Backes, K.R. Paton, D. Hanlon, S. Yuan, M.I. Katsnelson, J. Houston, et al., Spectroscopic metrics allow in-situ measurement of mean size and thickness of liquid-exfoliated few-layer graphene nanosheets, *Nanoscale* 8 (7) (2016) 4311–4323, <https://doi.org/10.1039/c5nr08047a>.
- [40] J.A. Morton, M. Khavari, L. Qin, B.M. Maciejewska, I. Tzanakis, A.V. Tyurnina, N. Grobert, D.G. Eskin, J. Mi, K. Porfyrakis, P. Prentice, New Insights into sonoexfoliation mechanisms of graphite: in situ high-speed imaging studies and acoustic measurements, *Mater. Today* (2021), <https://doi.org/10.1016/j.mat-tod.2021.05.005>. In press.
- [41] V.I. Il'ichev, *Proc Akust Inst Akad Nauk SSSR* 6 (1969) 16–29.
- [42] V. Belova, D.A. Gorin, D.G. Shchukin, H. Mohwald, *Angew. Chem. Int. Ed.* 49 (39) (2010) 7129–7133.
- [43] M. Petkovšek, M. Hočvar, M. Dular, Visualization and measurements of shock waves in cavitating flow, *Exp. Therm. Fluid Sci.* 119 (10) (2020) 110215, <https://doi.org/10.1016/j.expthermfluidsci.2020.110215>.
- [44] R. Feng, Y. Zhao, C. Zhu, T.J. Mason, Enhancement of ultrasonic cavitation yield by multi-frequency sonication, *Ultrason. Sonochem.* 9 (5) (2002) 231–236, [https://doi.org/10.1016/S1350-4177\(02\)00083-4](https://doi.org/10.1016/S1350-4177(02)00083-4).
- [45] E. Neppiras, Acoustic cavitation, *Phys. Rep.* 61 (3) (1980) 159–251, [https://doi.org/10.1016/0370-1573\(80\)90115-5](https://doi.org/10.1016/0370-1573(80)90115-5).
- [46] S. Kumar, C. Brennen, Harmonic cascading in bubble clouds, June, in: *International Symposium on Propulsors Cavitation*, 1992, pp. 22–25. Hamburg, Germany, <https://resolver.caltech.edu/CaltechAUTHORS:KUMpc92>.
- [47] O.V. Rudenko, S.I. Soluyan, *Theoretical Foundation of Nonlinear Acoustics*, Plenum Publishing Corporation, New York, 1977 (Chapter 5).